

## A GENERALIZATION OF THE SOBOLEV METHOD FOR FLOWS WITH NONLOCAL RADIATIVE COUPLING

G. B. RYBICKI

Center for Astrophysics

AND

D. G. HUMMER\*

Joint Institute for Laboratory Astrophysics, National Bureau of Standards and University of Colorado, Boulder

Received 1977 May 13; accepted 1977 July 15

### ABSTRACT

The Sobolev, or escape-probability, method for solving radiative transfer problems in moving atmospheres is generalized to treat flows in which the line-of-sight component of the flow velocity is not monotonic; for these cases the purely local nature of the approximation is lost, and radiative coupling between distant parts of the atmosphere must be taken into account. The method is formulated for a general three-dimensional flow. For spherically symmetric cases in which the relative projected flow velocity on a line of sight goes through zero 2, 3, . . . ,  $N$  times, an integral equation for the source function is obtained. In the simplest nontrivial case when  $N = 2$ , it is shown that the normalization of the kernel is such that an iterative solution of the integral equation always converges rapidly. For spherically symmetric flows with  $N = 2$ , the kernel of the integral equation is expressed in closed form. Extensive numerical results for inverse power-law velocity fields are presented to illustrate the magnitude of the coupling between different parts of the atmosphere. Errors in the magnitude of the flux peak of 50% or larger are readily made if this coupling is neglected.

*Subject headings:* line formation — radiative transfer

### I. INTRODUCTION

The concept of a "constant velocity surface," on which the line-of-sight projection of the flow velocity has a specified value has been extremely useful in discussing radiative transfer in spectral lines in gaseous bodies moving with velocity gradients. When the flow speed is much larger than the mean thermal speed of the gas, radiation at each frequency as seen by a fixed observer comes primarily from a unique mathematical surface. For certain important configurations, such as accelerating outflows (mathematically equivalent to decelerating inflows), each line of sight intersects any surface no more than once. Such situations can be treated by the approximate escape-probability method, due originally to Sobolev (1947, 1957) and extended by Castor (1970), Lucy (1971), and Rybicki (1970), and by direct numerical solutions of the transfer equation in the comoving frame of the gas, using methods developed by Noerdlinger and Rybicki (1974) for planar systems and by Mihalas, Kunasz, and Hummer (1975, 1976*a, b, c*) for spherical geometry.

Unfortunately, for a number of important astrophysical problems, gas flows are encountered for which the projection of the flow velocity on the line of sight is not necessarily monotonic, so that the constant velocity surfaces can intersect some lines of sight more than once; the material at these points of intersection can absorb and emit radiation of the same frequency and are thus radiatively coupled. Examples and discussion of this problem have been given in a review by Hummer (1976). Included in this class are accelerating inflows, associated, for example, with the collapse of interstellar clouds under certain conditions, decelerating outflows proposed recently by Kuan and Kuhi (1975) for the atmosphere of P Cygni, and differentially rotating stellar envelope, as encountered in Be stars. Because of the radiative coupling between distant parts of the same velocity surface, the escape-probability method loses its purely local nature, and the very large system of algebraic equations encountered in the numerical methods assumes a sufficiently complex structure that the highly efficient algorithm developed for the uncoupled problem is no longer applicable.

In this paper we derive expressions, in the spirit of the escape-probability method, that specify the source function for a completely general geometrical configuration and flow velocity field. These results are expressed in terms of an integral equation for configurations in which a surface is intersected an arbitrary number of times. An extensive development and illustrative numerical results are given for cases in which just two intersections occur. In this case an iterative solution of the integral equation is shown to converge very rapidly for all values of the

\* Staff Member, Quantum Physics Division, National Bureau of Standards.

atmospheric parameters. We expect that  $\Lambda$ -iteration will remain a useful method of solution for other geometric configurations. In spherically symmetric flows we obtain an important new representation of the kernel of the integral equation in closed form. Numerical solutions are obtained for a wide variety of situations, and are compared with results obtained by neglecting the radiative coupling, and with another purely local approximation proposed by Grachev and Grinin (1975).

However, we wish to stress that flows of the type discussed here, with the smallest flow speeds at the largest radii, are intrinsically less favorable for the application of the Sobolev method than are those in which the smallest speeds are found at small radii. Because the approximation is at its worst in a relatively large fraction of the gas volume, it is important for the prospective user to determine those parts of the line profile that are liable to be most adversely affected.

After the main results of the present paper had been obtained, we learned of the work of Marti and Noerdlinger (1977), who have presented a different method based on the same physical ideas; their work is limited to spherically symmetric flows with two intersections. Our method is more general and has distinct advantages in application. More recently, the paper of Grachev and Grinin (1975) has come to our attention. Although they have anticipated much of our conceptual and analytical development of the spherical case, they did not proceed to the integral equation (50) in radial coordinates, nor have they considered more than two intersections of a surface.

## II. THEORY

In this section we extend the escape-probability method to situations in which rays can intersect a velocity surface more than once. The present discussion is applicable to three-dimensional geometries and flow fields, although our most explicit results are limited to spherical symmetry. No attempt has been made to treat maser transitions. Applications of the more general results to models with axial symmetry are under way.

### *a) The Transfer Equation for Moving Media*

The transfer equation for a two-level atom in a three-dimensional moving medium has been discussed in detail by Rybicki (1970). It can be written

$$\mathbf{n} \cdot \nabla I(\mathbf{r}, \mathbf{n}, \nu) = -k(\mathbf{r}) \phi \left[ \nu - \frac{\nu_0}{c} \mathbf{n} \cdot \mathbf{v}(\mathbf{r}) \right] [I - S]. \quad (1)$$

$I(\mathbf{r}, \mathbf{n}, \nu)$  is the specific intensity at point  $\mathbf{r}$  in direction defined by the unit vector  $\mathbf{n}$  and at frequency  $\nu$ , and  $\mathbf{v}(\mathbf{r})$  is the material velocity field. The quantity

$$k(\mathbf{r}) = \frac{h\nu_0}{4\pi} B_{12} n_1(\mathbf{r}) \quad (2)$$

is the integrated line opacity, where  $\nu_0$  is the line-center frequency,  $B_{12}$  is the Einstein coefficient, and  $n_1$  is the population of the lower level (stimulated emission has been neglected). The speed of light and Planck's constant are given their usual designations,  $c$  and  $h$ .

The line profile function  $\phi(\mathbf{r}, \nu)$  has the frequency normalization

$$\int_0^\infty d\nu \phi(\mathbf{r}, \nu) = 1. \quad (3)$$

We shall generally suppress the explicit  $\mathbf{r}$ -dependence of the profile in our notation and simply write  $\phi(\nu)$ .

For complete redistribution the source function is

$$S(\mathbf{r}) = [1 - \epsilon(\mathbf{r})] \bar{J}(\mathbf{r}) + \epsilon(\mathbf{r}) B(\mathbf{r}), \quad (4)$$

where  $\epsilon$  is the ratio of collisional to total de-excitation rates from the upper level.  $B$  is the Planck function at frequency  $\nu_0$  and at the local electron temperature at point  $\mathbf{r}$ .

The integrated mean intensity is defined as

$$\bar{J}(\mathbf{r}) = \frac{1}{4\pi} \int d\Omega \int_0^\infty d\nu \phi \left[ \nu - \frac{\nu_0}{c} \mathbf{n} \cdot \mathbf{v}(\mathbf{r}) \right] I(\mathbf{r}, \mathbf{n}, \nu). \quad (5)$$

The first integral is over all solid angles of  $\mathbf{n}$ :  $d\Omega \equiv d\Omega(\mathbf{n})$ . A related quantity is the vector

$$\bar{H}(\mathbf{r}) = \frac{1}{4\pi} \int d\Omega \mathbf{n} \int_0^\infty d\nu \phi \left[ \nu - \frac{\nu_0}{c} \mathbf{n} \cdot \mathbf{v}(\mathbf{r}) \right] I(\mathbf{r}, \mathbf{n}, \nu). \quad (6)$$

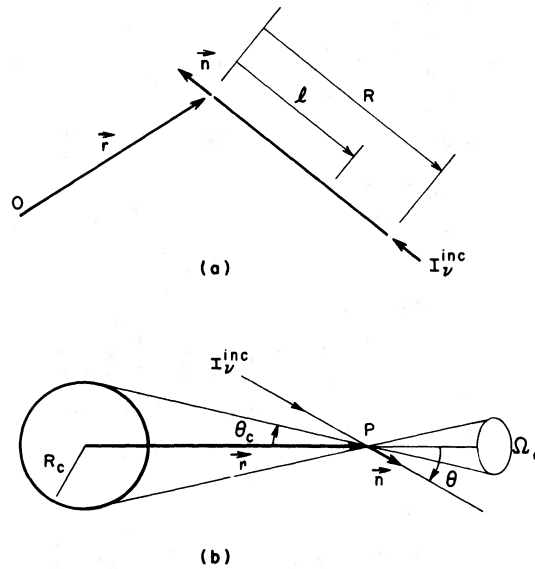


FIG. 1.—(a) Geometry of variables appearing in the formal solution, eq. (8); (b) geometry of the variables entering the calculation of  $\bar{J}$  for a single surface.

The radiation force per unit volume  $\mathcal{F}$  due to line photons is given in terms of  $\bar{H}$  by

$$\mathcal{F}(\mathbf{r}) = \frac{4\pi k(\mathbf{r})}{c} \bar{H}(\mathbf{r}). \quad (7)$$

We have assumed for simplicity that continuous absorption outside the line is negligible. Such absorption could be treated by a straightforward extension of the present methods.

The formal solution of the transfer equation (1) can be written for the intensity at an arbitrary point  $\mathbf{r}$  and direction  $\mathbf{n}$ :

$$I(\mathbf{r}, \mathbf{n}, \nu) = \int_0^R dl k(\mathbf{r} - \mathbf{n}l) \phi \left[ \nu - \frac{\nu_0}{c} \mathbf{n} \cdot \mathbf{v}(\mathbf{r} - \mathbf{n}l) \right] S(\mathbf{r} - \mathbf{n}l) \exp \left\{ - \int_0^l dl' k(\mathbf{r} - \mathbf{n}l') \phi \left[ \nu - \frac{\nu_0}{c} \mathbf{n} \cdot \mathbf{v}(\mathbf{r} - \mathbf{n}l') \right] \right\} \\ + I_v^{\text{inc}} \exp \left\{ - \int_0^R dl' k(\mathbf{r} - \mathbf{n}l') \phi \left[ \nu - \frac{\nu_0}{c} \mathbf{n} \cdot \mathbf{v}(\mathbf{r} - \mathbf{n}l') \right] \right\}. \quad (8)$$

The variable of integration  $l$  is the distance backwards along the ray passing through  $\mathbf{r}$  with direction  $\mathbf{n}$  (see Fig. 1a). The limit  $R$  is the distance at which an incident intensity  $I_v^{\text{inc}}$  is specified. In the physical problems to be treated here, this incident intensity is either specified at infinity (usually  $I = 0$ ) or as a prescribed radiation field on an appropriate stellar-like surface, which will be referred to as the *core*. It will be convenient for certain of the general derivations in the next section to make other choices for  $R$  as well.

#### b) The Sobolev Approximation

When the velocity gradients in the medium are sufficiently large, the above equations simplify considerably, as was first recognized by Sobolev (1947, 1957). We shall refer to the collection of results obtained by Sobolev and subsequent investigators as “the Sobolev method,” and restrict use of the expression “escape-probability method” to those special cases which lead to a purely local theory that approximates the effects of transfer by escape probability functions.

The effect of a large velocity gradient can be seen in the formal solution (8). The argument of the profile function  $\phi$  becomes a function of the distance along the ray, and, because the profile function is typically very narrow, it behaves like a  $\delta$ -function in the variable  $l$  (or  $l'$ ). This gives the intensity field within the medium a very simple behavior: Along a given ray the intensity at frequency  $\nu$  does not change at all, except at certain discrete *resonance points*, where the material has just the right Doppler shift to allow it to absorb and emit at frequency  $\nu$ . These points occur wherever the line-of-sight velocity  $v_l \equiv \mathbf{v} \cdot \mathbf{n}$  satisfies the resonance condition

$$(\nu - \nu_0)/\nu_0 = v_l/c, \quad (9)$$

which is found by setting the argument of  $\phi$  equal to  $\nu_0$ . Therefore, the problem of determining the intensities reduces to the simpler one of determining the variation of intensity in the neighborhood of a single resonance point. This is the essence of the Sobolev approximation.

The validity of the above physical picture depends on the sharpness of the resonance region. Its width  $\Delta l$  can be estimated by assuming that the gradient of  $v_i$  is constant over the region. Then differentiation of equation (9) yields

$$\Delta l = \frac{c}{\nu_0} \frac{\Delta \nu}{|dv_i/dl|}, \quad (10)$$

where  $\Delta \nu$  is the width of the profile function. Let us estimate  $|dv_i/dl| \approx v_0/l_0$ , where  $v_0$  is a typical velocity and  $l_0$  is a typical length scale in the medium. Assuming that the line width is due to Doppler broadening, then  $\Delta \nu = \nu_0 u_{\text{th}}/c$ , where  $u_{\text{th}}$  is the thermal (plus turbulent) velocity. It follows that

$$\Delta l/l_0 \approx u_{\text{th}}/v_0. \quad (11)$$

Therefore, the resonance regions will be relatively sharp when the macroscopic velocities are much larger than thermal; for this reason the Sobolev approximation is sometimes called the *supersonic approximation*.

### c) Two Fundamental Results

The behavior of the intensity near a resonant point will now be investigated. For this purpose it is useful to distinguish between quantities that vary on a "slow" scale, of the order of typical macroscopic scales, and those that vary on a "fast" scale, of the order of the width of the resonance region given by equation (10). When dealing with phenomena on the fast scale all slow-scale quantities, except the velocities, will be regarded as constant. The velocities need to be expanded up to first order, because it is just the variation of the velocities that gives rise to the effects we seek.

Suppose that point  $\mathbf{r}$  is in the neighborhood of a resonant point. By choosing the reference distance  $R$  to be small on the slow scale, but large on the fast scale, we ensure that only one resonant point contributes to the integrals in equation (8). The quantity  $I_v^{\text{inc}}$  then takes the (constant) value of the intensity before the radiation passes through the given resonant region.

We shall assume that the level populations of the given species varies on the slow scale only. This assumption will be justified *a posteriori*. Then the functions  $k$  and  $S$  can be taken outside the integrals in equation (8) by setting  $l = 0$  or  $l' = 0$ .

The velocities are expanded up to first order in  $l$ :

$$v_i(\mathbf{r} - \mathbf{n}l) = v_i(\mathbf{r}) - \sum_j n_j \frac{\partial v_i(\mathbf{r})}{\partial r_j} l. \quad (12)$$

An obvious tensor notation has been adopted here. Then

$$\mathbf{n} \cdot \mathbf{v}(\mathbf{r} - \mathbf{n}l) = \mathbf{n} \cdot \mathbf{v}(\mathbf{r}) - Q(\mathbf{r}, \mathbf{n})l, \quad (13)$$

where  $Q$  is a quadratic form in the components of the direction vector  $\mathbf{n}$ :

$$Q(\mathbf{r}, \mathbf{n}) = \sum_i \sum_j n_i n_j \frac{\partial v_i}{\partial v_j} = \sum_i \sum_j n_i n_j e_{ij} = \frac{dv_i}{dl}; \quad (14)$$

$Q$  is precisely what we had previously called  $dv_i/dl$ . The antisymmetric part of  $dv_i/\partial r_j$  does not contribute to  $Q$ , so that  $e_{ij}$  can be taken to be the symmetric rate-of-strain tensor:

$$e_{ij} \equiv \frac{1}{2} \left( \frac{\partial v_i}{\partial r_j} + \frac{\partial v_j}{\partial r_i} \right). \quad (15)$$

Expressions for the components of  $e_{ij}$  in several common coordinate systems are given, for example, in Batchelor (1967; Appendix 2).

Substituting these results into equation (8), we obtain

$$\begin{aligned} I(\mathbf{r}, \mathbf{n}, \nu) = & kS \int_0^R dl \phi \left[ \nu - \frac{\nu_0}{c} (\mathbf{n} \cdot \mathbf{v} + Ql) \right] \exp \left\{ -k \int_0^l dl' \phi \left[ \nu - \frac{\nu_0}{c} (\mathbf{n} \cdot \mathbf{v} + Ql') \right] \right\} \\ & + I_v^{\text{inc}} \exp \left\{ -k \int_0^R dl' \phi \left[ \nu - \frac{\nu_0}{c} (\mathbf{n} \cdot \mathbf{v} + Ql') \right] \right\}, \end{aligned} \quad (16)$$

where the quantities  $k$ ,  $S$ ,  $v$ , and  $Q$  are to be evaluated at  $r$ . Equation (16) will now be subjected to a series of transformations in order to derive the desired results. These results could be achieved more simply by one single transformation, but we believe each step in the present approach adds considerable insight.

In order to emphasize the dependence of this result on the fast scale, we first introduce new dimensionless distance and frequency variables:

$$\lambda = \frac{l}{\Delta l}, \quad \xi = \frac{\nu - (\nu_0/c)\mathbf{n} \cdot \mathbf{v}}{\Delta\nu}, \quad (17)$$

where  $\Delta l$  is given by equation (10) and  $\Delta\nu$  is some characteristic width of the line profile (say, its Doppler width). In addition we define the profile function

$$\varphi(\xi) = \Delta\nu\phi(\xi\Delta\nu), \quad (18)$$

which has the normalization

$$\int_{-\infty}^{\infty} \varphi(\xi)d\xi = 1. \quad (19)$$

The characteristic variations of this profile occur when  $\xi$  changes by order unity. The range of  $\xi$  can be taken to be  $-\infty$  to  $+\infty$ .

Details of the subsequent derivations depend on the sign of  $Q$ . We shall assume  $Q > 0$ , but the important results will be stated in a form valid for all  $Q$ . With these new variables equation (16) becomes

$$I = S\tau \int_0^{\infty} d\lambda\varphi(\xi - \lambda) \exp\left\{-\tau \int_0^{\lambda} d\lambda'\phi(\xi - \lambda')\right\} + I_v^{\text{inc}} \exp\left\{-\tau \int_0^{\infty} d\lambda'\varphi(\xi - \lambda')\right\}, \quad (20)$$

where

$$\tau \equiv k \frac{\Delta l}{\Delta\nu} = \frac{kc}{\nu_0|Q|} \quad (21)$$

is the total optical thickness of the velocity surface at point  $r$  measured in direction  $\mathbf{n}$ . The upper limits on two of the integrals in equation (20) should actually be  $R/\Delta l$ , but they have been replaced by  $\infty$ , since  $R \gg \Delta l$ .

The appearance of the quantities

$$t \equiv \xi - \lambda, \quad t' \equiv \xi - \lambda' \quad (22)$$

suggests that a further change of variables be made:

$$I = S\tau \int_{-\infty}^{\xi} dt\varphi(t) \exp\left\{-\tau \int_t^{\xi} dt'\phi(t')\right\} + I_v^{\text{inc}} \exp\left\{-\tau \int_{-\infty}^{\xi} dt'\varphi(t')\right\}. \quad (23)$$

We note that the variable  $t$  contains the spatial and frequency variables weighted equally, showing that changes in frequency and distance on the fast scale near a resonance point produce similar effects. This circumstance arises because the intensities depend only on the position relative to the resonance point, and this can be changed by varying either position or frequency, which moves the velocity surface.

A final change to the variable of integration

$$w(t) \equiv \int_{-\infty}^t dt'\varphi(t') \quad (24)$$

yields the result

$$I(\mathbf{r}, \mathbf{n}, \nu) = S\{1 - \exp[-\tau w(\xi)]\} + I_v^{\text{inc}} \exp[-\tau w(\xi)]. \quad (25)$$

Here  $\tau w(\xi)$  is the optical depth to a particular point within the resonance region, so that  $w(\xi)$  represents a normalized optical depth scale varying between 0 and 1. The limit  $\xi \rightarrow -\infty$  describes the side of the region on which the incident intensity  $I_v^{\text{inc}}$  falls. Let us define  $I_v^{\text{emg}}$  as the limit of  $I$  as  $\xi \rightarrow +\infty$ ; this is the intensity that emerges from the resonance region. Then from equation (25),

$$I_v^{\text{emg}} = I_v^{\text{inc}}e^{-\tau} + S(1 - e^{-\tau}). \quad (26)$$

This fundamental equation solves the problem of determining the variation of intensities on the slow scale: The intensity remains constant along a ray until it encounters a resonance point; it then suffers a discontinuous change governed by equation (26); and it subsequently remains constant at this new value until it escapes the medium

or encounters another resonance point. In the latter case equation (26) is applied again, using  $(I_\nu^{\text{inc}})_2 = (I_\nu^{\text{emg}})_1$ , where the subscripts refer to the first and second resonance points.

Another important use of equation (25) is to find the frequency integral of the intensity, weighted by the profile function

$$\bar{I}(\mathbf{r}, \mathbf{n}) = \int_0^\infty d\nu \phi \left[ \nu - \frac{\nu_0}{c} \mathbf{n} \cdot \mathbf{v}(\mathbf{r}) \right] I(\mathbf{r}, \mathbf{n}, \nu). \quad (27)$$

This quantity is important in determining the local excitation of the material and the radiation force, as in equations (5) and (6). The slow-scale behavior of the intensity is not sufficient to determine  $\bar{I}$ , because the integral of the product of a step function and a  $\delta$ -function is essentially indeterminate. We must evaluate it by changing to the fast variables, using equation (26):

$$\bar{I}(\mathbf{r}, \mathbf{n}) = \int_{-\infty}^\infty d\xi \varphi(\xi) \{ S [ 1 - e^{-\tau w(\xi)} ] + I_\nu^{\text{inc}} e^{-\tau w(\xi)} \}. \quad (28)$$

Introducing  $w(\xi)$  as the variable of integration, we obtain

$$\bar{I}(\mathbf{r}, \mathbf{n}) = S \left[ 1 - \frac{1 - e^{-\tau}}{\tau} \right] + I_\nu^{\text{inc}} \frac{1 - e^{-\tau}}{\tau}. \quad (29)$$

The  $\delta$ -function nature of the profile function implies that  $I_\nu^{\text{inc}}$  should be evaluated at  $\nu = \bar{\nu}$ , where

$$\bar{\nu} = \nu_0 + \frac{\nu_0}{c} \mathbf{n} \cdot \mathbf{v}(\mathbf{r}).$$

Physically, this is the line-center frequency Doppler shifted by motion of the medium along the line of sight.

Equations (26) and (29) are fundamental equations of the Sobolev approximation as applied to the complete redistribution case. These results are independent of the profile function, as first found by Sobolev (1957) in the plane-parallel case. We remark that these results also are valid for  $Q < 0$ , as long as  $\tau$  is defined in terms of the absolute value of  $Q$ , as in equation (21).

An interesting property of these equations appears when the velocity field is reversed, that is, when  $\mathbf{v}(\mathbf{r})$  is replaced by  $-\mathbf{v}(\mathbf{r})$ . Since  $\tau$  depends only on the absolute value of  $Q$ , it will not change, and the source function will remain the same. The frequency dependence of the intensities will simply change by a reflection in the line center, so that the blue wing behavior becomes the red wing behavior, and vice versa. This property is convenient in that it allows us to treat an expanding medium and then to deduce the corresponding properties of a contracting medium.

#### d) Velocity Surfaces

It is clear from the preceding that it is of crucial importance for the Sobolev approximation to locate the resonance points along each ray. A convenient way of representing these locations is through the concept of *velocity surfaces*. There are two types of velocity surfaces of particular utility, the *common-direction* velocity surfaces and the *common-point* velocity surfaces.

The common-direction (CD) velocity surfaces are defined as follows: Consider all rays passing through the medium that have the same direction, such as would be seen by a distant observer. For a given frequency  $\nu$  the resonance points along these rays, determined from equation (9), will all lie on a certain two-dimensional surface, all points of which have the same projected line-of-sight velocity relative to the observer. These are the velocity surfaces referred to in the Introduction, and are particularly useful in determining the observed intensities and fluxes, since they show immediately what parts of the medium can contribute to observations at frequency  $\nu$ . Sometimes these surfaces are called *surfaces of constant radial velocity*.

In the very simplest cases these velocity surfaces are *single*, that is, each ray intersects it at most once. This implies that there is at most one resonance pointing along any ray. However, in this paper we shall be particularly interested in cases where multiple intersections can occur. If two (but no more) resonance points exist along some rays, we say the surfaces are *double*. Higher multiplicities for surfaces can also be defined in similar fashion, but our primary interest will be in the double surface case.

In the multiple intersection case another kind of velocity surface can be defined as follows: Consider all rays passing through a point  $\mathbf{r}$ , and determine along each ray of direction  $\mathbf{n}$  all points  $\mathbf{r}'$  in resonance with  $\mathbf{r}$ , that is, such that the line-of-sight velocity is the same at  $\mathbf{r}$  and  $\mathbf{r}'$ :

$$\mathbf{n} \cdot \mathbf{v}(\mathbf{r}) = \mathbf{n} \cdot \mathbf{v}(\mathbf{r}'), \quad \mathbf{n} |\mathbf{r}' - \mathbf{r}| = \mathbf{r}' - \mathbf{r}. \quad (30)$$

These two equations are equivalent to the single one

$$(\mathbf{r} - \mathbf{r}') \cdot [\mathbf{v}(\mathbf{r}) - \mathbf{v}(\mathbf{r}')] = 0, \quad (31)$$

which says simply that the relative velocity between  $\mathbf{r}$  and  $\mathbf{r}'$  has no component along the line of sight. All such points  $\mathbf{r}'$  lie on a two-dimensional surface, which must pass through  $\mathbf{r}$ , since  $\mathbf{r}' = \mathbf{r}$  satisfies the equation. Grachev and Grinin (1975) call these  $s$ -surfaces, but we prefer the term *common-point* (CP) velocity surfaces. Note that CP surfaces are labeled by the spatial point used in their construction. This contrasts with the CD surfaces, which are labeled by a direction and a frequency. CP surfaces are particularly useful in describing the radiative coupling of different parts of the medium when multiple resonance points are present, since they show immediately what parts of the medium can interact with a given point.

The geometry of these velocity surfaces depends solely on the velocity field  $\mathbf{v}(\mathbf{r})$ , and in general can be quite complicated. Therefore it is of great interest to have a simple criterion for deciding when the velocity surfaces will be single. First note that if the line-of-sight velocity along every ray is a monotonic function of distance, then there can be at most one resonance point, and the surfaces will be single. Since  $dv_i/dl = Q$  is a quadratic form in the components of  $\mathbf{n}$ , a *sufficient* condition that the surfaces be single is that the rate-of-strain tensor  $e_{ij}$  be everywhere positive definite, or everywhere negative definite. An equivalent statement is that the three principal values of the tensor  $e_{ij}$  must be of the same sign everywhere. Physically, this can be understood as saying that the medium must be in a general state of expansion or a general state of contraction.

We should now like to investigate the extent to which this criterion is also necessary. Note that if  $Q$  is indefinite at any point, say  $\mathbf{r}_0$ , there will be directions for which  $Q = 0$ . Then typically there will be a double velocity surface for neighboring frequencies on one side of the resonant frequency. This argument would fail if the second derivative of  $v_i$  also vanished at  $\mathbf{r}_0$ . However, if  $Q$  is indefinite at  $\mathbf{r}_0$ , it will be indefinite in a neighborhood of  $\mathbf{r}_0$ , and it would require a rather special velocity law to have the second derivatives vanish everywhere within this neighborhood. (Such special examples do exist—e.g.,  $v_i = \sum_j e_{ij} r_j$ , with  $e_{ij}$  a constant, indefinite tensor.) Therefore, in practice we shall regard the above condition of definitions as both a necessary and a sufficient condition for single velocity surfaces.

The case of radial flow with spherical symmetry is a very important one, and we shall now consider the special simplifications that obtain in this case. The velocity field is specified by a single function of the radial distance  $v(r)$ ; positive  $v$  implies outflow; negative  $v$ , inflow. The rate-of-strain tensor (Batchelor 1967) has one principal axis in the radial direction with principal value  $v'(r)$ , and has the two others in tangential directions, each with the common principal value  $v(r)/r$ . These are called, respectively, the *radial* and the *tangential velocity gradients*.

By the above criterion the surfaces will be single if  $v'(r)$  and  $v(r)$  have the same sign for all  $r$ . For stationary flows, this implies outward acceleration, or, as we shall say, *accelerated outflow* or *decelerated inflow*. If the flow is not stationary, no such conclusions about accelerations can be drawn; however, for convenience we shall adopt the same terms for nonstationary flows as well, recognizing that they may be misnomers in such cases.

Multiple surfaces occur whenever  $v'(r)$  and  $v(r)$  have opposite signs for any range of  $r$ . In stationary flows, this occurs in regions of inward acceleration, or as we shall say, *decelerated outflow* or *accelerated inflow*. In subsequent sections we shall derive some general results applicable to double surfaces. Surfaces of higher multiplicity generally have to be treated on a case-by-case basis; a brief discussion of this problem is given in § IIg.

#### e) Single Velocity Surfaces

We shall now derive the complete set of equations for the Sobolev method when the velocity surfaces are single. No specific assumptions about the geometry need to be made, and it can be taken as a general three-dimensional medium with arbitrary velocity field, except of course that the conditions for single-velocity surfaces must be met. In addition we shall assume that there is a stellar-like surface (the “core”), which emits a continuum radiation field of specific intensity  $I_c$  near the relevant line frequencies, and which exhibits no limb-darkening. These latter assumptions are chosen for simplicity, and they could be easily modified.

The basic equation to determine the state of excitation of the material is equation (29). At any point  $\mathbf{r}$  the rays with direction  $\mathbf{n}$  that originate on the core lie within the solid angle  $\Omega_c$ . All others originate at infinity, where we assume no incident intensity. Therefore,

$$\begin{aligned} I_\nu^{\text{inc}} &= I_c, & \mathbf{n} \in \Omega_c, \\ &= 0, & \mathbf{n} \notin \Omega_c, \end{aligned} \quad (32)$$

Substituting (32) into equation (29) and integrating over all solid angles we obtain

$$\bar{J}(\mathbf{r}) = [1 - \beta(\mathbf{r})]S(\mathbf{r}) + \beta_c(\mathbf{r})I_c, \quad (33)$$

where the definition of  $\bar{J}$  in equation (5) has been used. The quantities  $\beta$  and  $\beta_c$  are given by

$$\beta(\mathbf{r}) = \frac{1}{4\pi} \int d\Omega \frac{1 - e^{-\tau}}{\tau} \quad (34)$$

and

$$\beta_c(\mathbf{r}) = \frac{1}{4\pi} \int_{\Omega_c} d\Omega \frac{1 - e^{-\tau}}{\tau}. \quad (35)$$

The dependence of  $\tau$  on  $\mathbf{n}$  is found through equations (14) and (21).

A similar expression can be derived for the quantity  $\bar{H}(\mathbf{r})$ , given in equation (6):

$$\bar{H}(\mathbf{r}) = \gamma_c(\mathbf{r})I_c, \quad (36)$$

where

$$\gamma_c(\mathbf{r}) = \frac{1}{4\pi} \int_{\Omega_c} d\Omega \mathbf{n} \frac{1 - e^{-\tau}}{\tau}. \quad (37)$$

Notice that a term proportional to  $S(\mathbf{r})$  does not appear in equation (36), as it does in equation (33), because the part of  $\bar{I}$  proportional to  $S$  is an even function of  $\mathbf{n}$ , and integration with the factor  $\mathbf{n}$  gives zero. Physically this means that the local contribution to the radiation force vanishes in this approximation. By accounting for the anisotropy of the diffuse radiation field, Sobolev (1957) and Castor (1974) obtain a nonzero contribution to the force that is proportional to  $dS/dr$ ; Castor discusses this point in some detail.

The source function can be determined by substituting equation (33) into equation (4). The result is

$$S(\mathbf{r}) = \frac{(1 - \epsilon)\beta_c I_c + \epsilon B}{\epsilon + (1 - \epsilon)\beta}. \quad (38)$$

This algebraic solution for the source function is expressed entirely in terms of known parameters evaluated at the given point  $\mathbf{r}$ . The absence of global radiative coupling for single velocity surfaces leads to a simple, locally determined solution. Since all quantities on the right-hand side vary only on the slow scale, the source functions and level populations also will vary only on the slow scale. This is the *a posteriori* justification for these assumptions made in deriving equation (16).

The quantity  $\beta$  is the *escape probability*, that is, the probability that an emitted photon will escape the local neighborhood of  $\mathbf{r}$  without suffering any absorption or scattering. A derivation of equation (34) using this physical interpretation was given by Rybicki (1970); his arguments were subsequently repeated by de Jong, Chu, and Dalgarno (1975). A similar interpretation can be given to  $\beta_c$  as the probability that a photon will escape the local neighborhood of  $\mathbf{r}$  and strike the core.

One notes that the geometry of the velocity surfaces has not entered into the discussion up to this point, except that these surfaces were single. In order to find the observed intensities and fluxes, however, this geometry is crucial. For every frequency  $\nu$  the CD surface is determined from equation (9). Then for each observed ray equation (26) is applied; the intensity  $I_\nu^{\text{inc}}$  is set equal to  $I_c$  for rays originating on the core, and to zero otherwise. Some rays may not intersect the velocity surface at all; such cases can be regarded as special cases of equation (26) with  $\tau = 0$ . In this way the observed intensities as a function of frequency and position in the plane of the sky are determined. In many cases the source will not be resolved, and then the only observed quantity of interest is the monochromatic flux  $F_\nu$ . For an observer at a large distance  $D$  from the source we have

$$F_\nu = \frac{1}{D^2} \int I_\nu dA, \quad (39)$$

where the region of integration is the area of a plane normal to the direction of observation.

For spherically symmetric flows these formulae can be simplified somewhat. Let us define the direction  $\mathbf{n}$  by the direction cosine of the ray with respect to the outward radial direction  $\mu = \cos \theta$  (see Fig. 1b). Let  $\theta_c$  be the half-angle subtended by the core as viewed from point  $\mathbf{r}$  and let  $\mu_c = \cos \theta_c$ . Then in equation (32) the conditions  $\mathbf{n} \in \Omega_c$  and  $\mathbf{n} \notin \Omega_c$  can be written  $\mu > \mu_c$  and  $\mu < \mu_c$ , respectively. The quantities  $\beta$  and  $\beta_c$  can be written

$$\beta(\mathbf{r}) = \frac{1}{2} \int_{-1}^{+1} d\mu \frac{1 - e^{-\tau}}{\tau} \quad (40)$$

and

$$\beta_c(\mathbf{r}) = \frac{1}{2} \int_{\mu_c}^{+1} d\mu \frac{1 - e^{-\tau}}{\tau}; \quad (41)$$

$\tau$  is determined by equation (14), and equation (21) becomes

$$Q = \mu^2 v'(r) + (1 - \mu^2) \frac{v(r)}{r}. \quad (42)$$

The vector  $\bar{H}$  is directed radially with magnitude

$$\bar{H} = \gamma_c I_c; \quad \gamma_c = \frac{1}{2} \int_{\mu_c}^{+1} d\mu \mu \frac{1 - e^{-\tau}}{\tau}. \quad (43)$$

If we use the usual impact parameter  $p$  to specify rays, where  $p = r(1 - \mu^2)^{1/2}$ , then the observed intensities can be conveniently given as functions of  $\nu$  and  $p$ . Then equation (39) becomes

$$F_\nu = \frac{2\pi}{D^2} \int_0^\infty dp p I_\nu^{\text{obs}}(p). \quad (44)$$

These equations for the single-surface, spherically symmetric case were first given by Castor (1970).

#### f) Double Velocity Surfaces

The presence of multiple velocity surface introduces the physical complication of radiative coupling between distant parts of the medium. Since this complication already appears for double velocity surfaces, it is natural to treat this case first before attacking the general case of multiple velocity surfaces. First we shall develop the theory for double velocity surfaces as far as possible for general geometry and flow fields. Then we shall consider the case of spherically symmetric flows and inverse power-law velocity laws.

##### i) General Theory

The two fundamental equations (26) and (29) can be easily written in forms suitable for double surfaces. For example, the intensity after passing through two surfaces is

$$I_\nu^{\text{emg}} = e^{-\tau} e^{-\tau'} I_\nu^{\text{inc}} + e^{-\tau} (1 - e^{-\tau'}) S' + (1 - e^{-\tau}) S, \quad (45)$$

where the primed and unprimed quantities respectively refer to the first and second surfaces traversed by the ray. This is simply proved by writing equation (26) for each surface and recognizing that the intensity emergent from the first is the intensity incident on the second. Similarly, the expression for  $\bar{I}$  can be written

$$\bar{I}(\mathbf{r}, \mathbf{n}) = e^{-\tau'} \frac{1 - e^{-\tau}}{\tau} I_\nu^{\text{inc}} + (1 - e^{-\tau'}) \frac{1 - e^{-\tau}}{\tau} S' + \left[ 1 - \frac{1 - e^{-\tau}}{\tau} \right] S. \quad (46)$$

Note that the resonance condition (30) implies that the value of  $\bar{\nu}$  is the same for the primed and the unprimed surface. Equations (45) and (46) apply to the case of single velocity surfaces as well, if in such cases it is agreed that  $\tau'$  should be set to zero, thereby recovering equations (26) and (29); this convention will be followed for the remainder of the paper. The various types of rays that can exist for double velocity surfaces are illustrated in Figure 2.

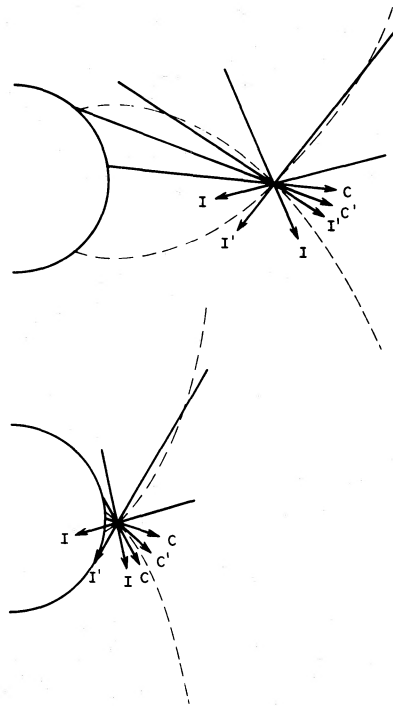


FIG. 2.—Illustration of common-point velocity surfaces (dashed lines) for  $\mu_c > \mu_{\text{crit}}$  (upper diagram) and for  $\mu_c < \mu_{\text{crit}}$  (lower diagram), where  $Q(\mu_{\text{crit}}) = 0$ . I denotes a ray originating at infinity, and C denotes a ray originating at the core. A prime indicates that a ray has intersected the velocity surface.

Again taking the incident boundary conditions of equation (32), we can integrate equation (46) over all solid angles to yield

$$\bar{J}(\mathbf{r}) = [1 - \beta(\mathbf{r})]S(\mathbf{r}) + \bar{\beta}_c(\mathbf{r})I_c + \frac{1}{4\pi} \int d\Omega (1 - e^{-\tau}) \frac{1 - e^{-\tau}}{\tau} S(\mathbf{r}'). \quad (47)$$

The right-hand member of this equation should be compared with that of equation (33). The first term is identical, as  $\beta(\mathbf{r})$  is defined exactly as in equation (34) and has the same interpretation as the escape probability. The second term is almost the same, except that  $\bar{\beta}_c$  is now defined by

$$\bar{\beta}_c = \frac{1}{4\pi} \int_{\Omega_c} d\Omega e^{-\tau'} \frac{1 - e^{-\tau}}{\tau}. \quad (48)$$

This contains a correction for possible absorption by the primed velocity surface. Such corrections occur for rays labeled  $c'$  in Figure 2. The third term is essentially new and represents the radiative coupling between material at  $\mathbf{r}$  and material at various other points  $\mathbf{r}'$  with which it is in resonance. These points  $\mathbf{r}'$  all lie on the CP velocity surface associated with point  $\mathbf{r}$ . An equivalent equation was derived and solved approximately by Grachev and Grinin (1975).

Formally we may write the integral in equation (47) as

$$\frac{1}{4\pi} \int d\Omega (1 - e^{-\tau}) \frac{1 - e^{-\tau}}{\tau} S(\mathbf{r}') = \int M(\mathbf{r}, \mathbf{r}') S(\mathbf{r}') d^3\mathbf{r}'. \quad (49)$$

The explicit form of the kernel function  $M(\mathbf{r}, \mathbf{r}')$  will not be exhibited here; suffice to say that it contains  $\delta$ -functions that make the integration over  $\mathbf{r}'$  effective only on the CP velocity surface associated with point  $\mathbf{r}$ . When equations (47) and (48) are used in equation (4), an integral equation determining the source function is obtained:

$$S(\mathbf{r}) = \frac{(1 - \epsilon) \int M(\mathbf{r}, \mathbf{r}') S(\mathbf{r}') d^3\mathbf{r}' + (1 - \epsilon)\bar{\beta}_c I_c + \epsilon\beta}{\epsilon + (1 - \epsilon)\beta}. \quad (50)$$

Such integral equations are commonly encountered in radiative transfer problems. The general character of the solution of such equations and its dependence on the various parameters is well understood (cf. Hummer and Rybicki 1970). A quantity of great importance in this regard is the normalization of the kernel function

$$\eta(\mathbf{r}) \equiv \int M(\mathbf{r}, \mathbf{r}') d^3\mathbf{r}'. \quad (51)$$

Since  $\eta$  is simply the value of the integrals (49) when  $S$  is set equal to unity, we also have

$$\eta(\mathbf{r}) = \frac{1}{4\pi} \int d\Omega (1 - e^{-\tau}) \frac{1 - e^{-\tau}}{\tau}. \quad (52)$$

An important bound on  $\eta$  can now be derived for the case of double velocity surfaces. If a ray does not intersect the velocity surface at the primed point before passing through  $\mathbf{r}$ , we set  $\tau' = 0$ , so that  $(1 - e^{-\tau}) = 0$ . Therefore, the integral in equation (52) need only be over the set of solid angles  $\Omega_2$  for which such intersections do occur. Since  $(1 - e^{-\tau}) < 1$ , we have

$$\eta < \frac{1}{4\pi} \int_{\Omega_2} d\Omega \frac{1 - e^{-\tau}}{\tau}. \quad (53)$$

Suppose that a ray with direction  $\mathbf{n}$  lies within  $\Omega_2$ ; that is, it does intersect the velocity surface before passing through  $\mathbf{r}$ . But then the oppositely directed ray ( $-\mathbf{n}$ ) cannot lie within  $\Omega_2$ , because this would imply three intersections along a single ray (remember  $\mathbf{r}$  itself lies on the surface). Since  $\tau$  is an even function of  $\mathbf{n}$ , it follows that the above integral is bounded by half the value of the integral taken over all solid angles. Noting the definition (34) for  $\beta$ , we have finally

$$0 < \eta < \frac{1}{2}\beta. \quad (54)$$

This has the physical interpretation that fewer than half the photons that escape the local neighborhood of a point can be reabsorbed by another part of the medium.

The nature of the solutions to the integral equation (50) depends on the normalization of the kernel  $M$  multiplied by the various parameters outside the integral:

$$\sigma \equiv \frac{1 - \epsilon}{\epsilon + (1 - \epsilon)\beta} \eta. \quad (55)$$

With the bound (54) it is easily shown that

$$0 < \sigma < \frac{1}{2}. \quad (56)$$

This has important implications for the numerical solution of the integral equation. A classic method of solution for such integral equations is  $\Lambda$ -iteration, which involves the substitution of an approximate source function into the right-hand side of equation (50) to obtain an improved source function on the left-hand side. The process is continued until convergence is obtained. The rate of convergence of  $\Lambda$ -iteration is roughly as powers of  $\sigma$ , so that it is very slow when  $\sigma$  is close to unity. However, the bound (56) shows that the rate of convergence will be at least as fast as powers of  $\frac{1}{2}$ , which implies that  $\Lambda$ -iteration will generally be a feasible method of solution for cases of double velocity surfaces. These general arguments were corroborated by our numerical results, which will be discussed in § III.

It should perhaps be pointed out that it is not necessary to construct the kernel function  $M(\mathbf{r}, \mathbf{r}')$  in order to use  $\Lambda$ -iteration, because the integral of the kernel with  $S$  could be evaluated by the angular integral in equation (48) as well. Another alternative procedure is the following: given an estimated source function, the intensity field can be easily constructed from the formal solution (26), and then  $\bar{J}$  can be found from an angular quadrature of  $\bar{I}$ , given by equation (29). Then an improved source function is found from equation (5). Any of these methods is equivalent to the  $\Lambda$ -iteration method, and the rate of convergence will be the same. The choice of method will depend upon the problem; for the case of spherically symmetric flow it is easiest to construct the kernel, as we shall show presently.

There have appeared in the literature two approximate methods for solving the integral equation (50) in spherical geometry. Kuan and Kuhi (1975) simply ignored the integral term, and so neglected the radiative coupling between points  $\mathbf{r}$  and  $\mathbf{r}'$ . Marti and Noerdlinger (1977) have called this the *disconnected approximation*. We shall denote the resulting source function by  $S_0$ . Grachev and Grinin (1975) set  $S(\mathbf{r}') = S(\mathbf{r})$  in the integral term, and so neglected the variation of the source function between points  $\mathbf{r}$  and  $\mathbf{r}'$ . We shall call this the *Grachev and Grinin approximation*, and denote the resulting source function by  $S_{GG}$ . These source functions are given explicitly by

$$S_0 = [\epsilon + (1 - \epsilon)\beta]^{-1}[(1 - \epsilon)\bar{\beta}_c I_c + \epsilon B], \quad (57)$$

$$S_{GG} = [\epsilon + (1 - \epsilon)(\beta - \eta)]^{-1}[(1 - \epsilon)\bar{\beta}_c I_c + \epsilon B]. \quad (58)$$

There is some ambiguity in the definition of  $\bar{\beta}_c$  here. In the spirit of the disconnected approximation perhaps one should use  $\beta_c$ , defined without the absorption factor  $e^{-\tau}$ . Thus we should have a further classification of these approximations using "corrected" or "uncorrected" values of  $\beta_c$ . However, we have found in our numerical studies that the absorption corrections are too small to make it worthwhile making these distinctions.

These source functions differ solely in their first factors. From the bound (54) we have  $\beta > \beta - \eta > \frac{1}{2}\beta$ , so that

$$\epsilon + (1 - \epsilon)\beta > \epsilon + (1 - \epsilon)(\beta - \eta) > \epsilon + \frac{1}{2}(1 - \epsilon)\beta > \frac{1}{2}[\epsilon + (1 - \epsilon)\beta]. \quad (59)$$

Therefore, we obtain the general result

$$S_0 < S_{GG} < 2S_0. \quad (60)$$

Detailed numerical comparisons of  $S_0$ ,  $S_{GG}$ , and the true source functions will be made in § III.

The result for  $\bar{H}$  can be found by multiplying equation (46) by  $\mathbf{n}$  and integrating:

$$\bar{H}(\mathbf{r}) = \bar{\gamma}_c I_c + \frac{1}{4\pi} \int_{\Omega_2} d\Omega \mathbf{n} (1 - e^{-\tau}) \frac{1 - e^{-\tau}}{\tau} S(\mathbf{r}'), \quad (61)$$

where

$$\bar{\gamma}_c = \frac{1}{4\pi} \int_{\Omega_c} d\Omega \mathbf{n} e^{-\tau} \frac{1 - e^{-\tau}}{\tau}. \quad (62)$$

The first term in equation (61) is similar to that of equation (36) except that  $\bar{\gamma}_c$  now has an absorption correction. The second term is new and represents the radiative coupling between the various parts of the medium. This term is clearly very important, since it can even change the *direction* of the radiative force. Thus the disconnected approximation is definitely not sufficient to discuss radiative forces, even qualitatively.

The calculation of the observed intensities and fluxes proceeds in very much the same way as described for the single surface case, except that the basic equation is now equation (45). In practice it may be just as easy to apply equation (26) twice. The observed flux is still given by equation (39). The construction of the CD velocity surfaces is the major difficulty here, but there is not much of a general nature that can be said about this. In a subsequent section a more detailed discussion of such surfaces will be given for the case of inverse power velocity laws in spherically symmetric flows.

ii) *Spherically Symmetric Flows*

The primary simplification here, aside from the reduction to a scalar variable  $r$ , is that many of the properties of the common point velocity surfaces can be analyzed quite completely. Equation (30) becomes

$$\mu v(r) = \mu' v(r'). \quad (63)$$

The constancy of the impact parameter  $p$  implies

$$r(1 - \mu^2)^{1/2} = r'(1 - \mu'^2)^{1/2}. \quad (64)$$

Therefore,

$$\mu^2 = \frac{(r'^2 - r^2)v^2(r')}{r'^2 v^2(r) - r^2 v^2(r')} \quad (65)$$

expresses  $\mu$  explicitly as a function of  $r$  and  $r'$ . Thus from equation (42)  $Q$  has the explicit form

$$Q = \frac{rv'(r)(r'^2 - r^2)v^2(r') + v(r)r'^2[v^2(r) - v^2(r')]}{r[r'^2 v^2(r) - r^2 v^2(r')]} \quad (66)$$

The expressions for  $\mu'$  and  $Q'$  are similar except that primed and unprimed variables are interchanged (the prime on  $v$  means differentiation and is not changed). With these results the quantities  $\tau$  and  $\tau'$  can be expressed explicitly in terms of  $r$  and  $r'$  through the relations

$$\tau = \frac{c}{v_0} \frac{k(r)}{|Q|}, \quad \tau' = \frac{c}{v_0} \frac{k(r')}{|Q'|} \quad (67)$$

Now the integral term in equation (50) can be written

$$\frac{1}{2} \int_{-1}^{+1} d\mu (1 - e^{-\tau}) \frac{1 - e^{-\tau'}}{\tau} S(r') = \int_{r_c}^{r_{\max}} K(r, r') S(r') k(r') r'^2 dr', \quad (68)$$

where  $r_c$  and  $r_{\max}$  are the inner and outer radii of the medium. The kernel  $K(r, r')$  is related to, but not the same as, the kernel  $M(r, r')$  introduced earlier. A straightforward calculation yields the result

$$\frac{d\mu}{dr'} = \frac{r'^2 Q(r', \mu')}{\{(r'^2 - r^2)[r'^2 v^2(r) - r^2 v^2(r')]\}^{1/2}} \quad (69)$$

By changing the variable of integration in equation (68) we obtain an explicit expression for the kernel function as a function of  $r$  and  $r'$ :

$$K(r, r') = \frac{c}{2v_0} \frac{1 - e^{-\tau}}{\tau} \frac{1 - e^{-\tau'}}{\tau'} \frac{1}{\{(r'^2 - r^2)[r'^2 v^2(r) - r^2 v^2(r')]\}^{1/2}} \quad (70)$$

This kernel function is symmetric in  $r$  and  $r'$ .

A similar kernel can be defined to express the quantity  $\bar{H}$ :

$$\begin{aligned} \bar{H} &= \bar{\gamma}_c I_c + \frac{1}{2} \int_{-1}^{+1} d\mu \mu (1 - e^{-\tau}) \frac{1 - e^{-\tau'}}{\tau} S(r') \\ &= \bar{\gamma}_c I_c + \int_{r_c}^{r_{\max}} L(r, r') S(r') k(r') r'^2 dr', \end{aligned} \quad (71)$$

where

$$\bar{\gamma}_c = \frac{1}{2} \int_{\mu_c}^1 d\mu \mu e^{-\tau} \frac{1 - e^{-\tau'}}{\tau} \quad (72)$$

and

$$L(r, r') = \frac{c}{2v_0} \frac{1 - e^{-\tau}}{\tau} \frac{1 - e^{-\tau'}}{\tau'} \frac{v(r')}{r^2 v^2(r') - r'^2 v^2(r)} \quad (73)$$

No absolute values appear here; for  $r > r'$  the contribution to  $\bar{H}$  is positive, and for  $r < r'$  it is negative.

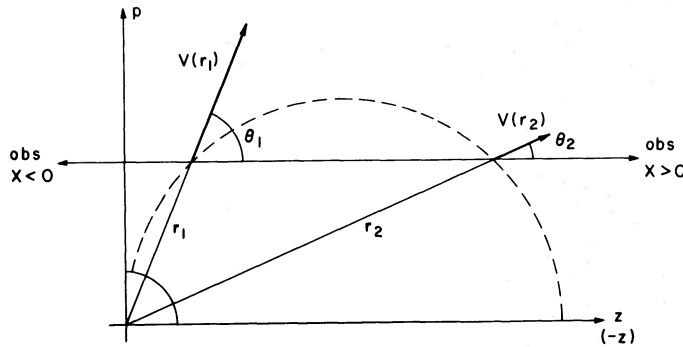


FIG. 3.—Geometry of CD velocity surface

The above expressions for  $K(r, r')$  and  $L(r, r')$  are new, and they show that for problems with double velocity surfaces it is possible to determine the source function and radiation force without ever having to consider the equation for the CP velocity surface (in general a transcendental equation). To find the observed intensities and fluxes, however, it is necessary to determine the CD velocity surfaces, as before.

We note finally that the escape probability  $\beta$  still has the form (40), while  $\bar{\beta}_c$  follows from equation (48):

$$\bar{\beta}_c = \frac{1}{2} \int_{\mu_c}^1 d\mu e^{-\tau} \frac{1 - e^{-\tau}}{\tau}. \quad (74)$$

iii) *Inverse Power-Law Velocities*

A prototype velocity law giving rise to double velocity surfaces is the inverse power law

$$v(r) = v_0 \left( \frac{r_0}{r} \right)^p, \quad \alpha > 0; \quad (75)$$

for convenience we take  $r_0 = r_c$ , the radius of the core, and  $v_0 = v(r_0)$ . This law was also treated by Marti and Noerdlinger (1977). The more general law treated by Grachev and Grinin (1975) is, in our notation,

$$v(r) = v_0 \left( a \frac{r_0}{r} + 1 - a \right)^\alpha. \quad (76)$$

The extra parameter  $a$  allows description of a velocity field with a terminal velocity as  $r \rightarrow \infty$ . For simplicity, we shall confine our attention solely to the law (75).

We shall investigate the cases  $\alpha = 1$  and  $\alpha = \frac{1}{2}$  in detail. We shall also assume that the conservation of particles applies to the ground state of the species in question,

$$n_1(r) = n_0 \left( \frac{r_0}{r} \right)^{2-\alpha}, \quad (77)$$

so that  $n_1 v r^2 = \text{const}$ . This assumption is not essential to our methods.

Let us investigate the common-direction surfaces. It is convenient to introduce a  $p$ - $z$  coordinate system, as in Figure 3. The intersections are determined by the equation

$$v(r) \cos \theta = \frac{c}{v_0} (v - v_0) \equiv x, \quad (78)$$

where  $x$  measures the frequency displacement from line center in velocity units. Note particularly that  $x > 0$  refers to material moving toward the observer. Using  $\cos \theta = [1 - (p/r)^2]^{1/2}$  and the velocity law (75), equation (78) can be put into the form

$$f(r) \equiv r^2 - \left( \frac{x}{v_0 r_0^\alpha} \right)^2 r^{2\alpha+2} = p^2. \quad (79)$$

The function  $f(r)$  vanishes at two points  $r = 0$  and  $r = r_0(v_0/x)^{1/\alpha}$ . Between these two points it is positive and concave downward, reaching a maximum value

$$p_{\max}^2 = \left[ \frac{v_0^2}{x^2(1+\alpha)} \right]^{1/\alpha} \frac{\alpha}{1+\alpha} r_0^2 \quad (80)$$

at

$$r_3 = (1 + \alpha)^{-1/2\alpha} \left( \frac{u_0}{x} \right)^{1/\alpha} r_0. \quad (81)$$

These properties imply that there are no roots for  $p > p_{\max}$ , and there are precisely two roots  $r_1$  and  $r_2$  for  $p < p_{\max}$ . This justifies our use of the inverse power law (75) as a prototype for double velocity surfaces.

Equation (79) can easily be solved by the Newton-Raphson method. For the special case  $\alpha = 1$  it is a quadratic in  $r^2$  and can be solved directly. For  $\alpha = \frac{1}{2}$  the equation is a cubic in  $r$ , and so could be solved directly, but we found it more convenient to solve this case by the Newton-Raphson method as well.

The case illustrated in Figure 3 is for  $\alpha = 1$  and for outflow ( $v_0 > 0$ ). The observer is taken to be at  $z \rightarrow \infty$ . For  $x > 0$  the velocity surface is as shown in the half-space  $z > 0$ . For  $x < 0$  the velocity surface would be in the half-space  $z < 0$ . We have taken advantage of the fact that for  $x < 0$  the surfaces are simply reflected in the plane  $z = 0$ , and have shown the observer's line of sight in this case to the left. A similar diagram would hold for inflow ( $v_0 < 0$ ) except that the meanings of  $x > 0$  and  $x < 0$  would be interchanged.

Let us now discuss the common-point velocity surfaces. They are determined by the solution of equation (65) for  $r'$  given  $r$  and  $\mu$ . For the case of the inverse power-law velocities with  $\alpha$  a half-integer or an integer, this equation is reducible to a polynomial equation in  $r'$ . But  $r' = r$  must be a root of this equation, since the CP surface passes through  $r$ , so the degree of the polynomial can be reduced by at least one by dividing by  $(r - r')$ . For instance, when  $\alpha = \frac{1}{2}$  or 1, the equation becomes quadratic in  $r'$ :

$$(r'^2 + rr' + r^2)\mu^2 = rr' + r^2, \quad \alpha = \frac{1}{2}; \quad (82)$$

$$(r^2 + r'^2)\mu^2 = r^2, \quad \alpha = 1. \quad (83)$$

As we have noted previously, however, it is possible to effect a complete solution to the transfer problem without having to solve these equations for the CP surfaces. Therefore we shall discuss them no further.

For inverse power-law velocities,  $Q$  may be conveniently expressed as

$$Q = \frac{v_0 r_0^\alpha}{r^{\alpha+1}} \tilde{Q}, \quad (84)$$

where

$$\tilde{Q} \equiv 1 - (1 + \alpha)\mu^2 = \alpha - (1 + \alpha)p^2/r^2. \quad (85)$$

Using equations (2), (21), and (77), we find

$$\tau = \tau_0 \left( \frac{r_0}{r} \right)^{1-2\alpha} \frac{1}{|\tilde{Q}|}, \quad (86)$$

where

$$\tau_0 = \frac{hcB_{12}r_0n_0}{4\pi v_0}. \quad (87)$$

The quantity  $\tau_0$  is the tangential ( $\mu = 0$ ) optical thickness of the velocity surface at the inner radius  $r_0$ , and is a convenient parameter to use in characterizing the problem. It can be related to the quantity  $\tau_0$  used by Marti and Noerdlinger (1977), which is the *radial* ( $\mu = 1$ ) optical thickness at the *outer* radius  $r_{\max}$ :

$$\tau_0 = \alpha \left( \frac{r_0}{r_{\max}} \right)^{2\alpha-1} (\tau_0)_{MN}. \quad (88)$$

We now give expressions for  $\tau(r, r')$  for use in the kernel functions  $K$  and  $L$ :

$$\tau(r, r') = \tau_0 \left| \frac{r'^2 + rr' + r^2}{(r' - r)(2r' + r)} \right|, \quad \alpha = \frac{1}{2} \quad (89)$$

$$\tau(r, r') = \tau_0 \left( \frac{r}{r_0} \right) \left| \frac{r'^2 + r^2}{r'^2 - r^2} \right|, \quad \alpha = 1. \quad (90)$$

The corresponding expressions for  $\tau'$  can be found by interchanging  $r$  and  $r'$ .

It is useful to have asymptotic expressions for  $\beta$  and  $\beta_c$  when the optical thickness  $\tau$  of the surface is large. This will occur when

$$\tau_0(r_0/r)^{1-2\alpha} \gg 1. \quad (91)$$

In this case  $(1 - e^{-\tau}) \approx 1$ , so that

$$\beta \sim \int_0^1 \frac{d\mu}{\tau} = \frac{1}{\tau_0} \left(\frac{r}{r_0}\right)^{1-2\alpha} \int_0^1 |(1 + \alpha)\mu^2 - 1| d\mu \sim \frac{1}{\tau_0} \left(\frac{r}{r_0}\right)^{1-2\alpha} \left[ \frac{4}{3\sqrt{1+\alpha}} + \frac{\alpha}{3} - \frac{2}{3} \right]. \quad (92)$$

Similarly

$$\bar{\beta}_c \sim \frac{\alpha}{4\tau_0} \left(\frac{r}{r_0}\right)^{1-2\alpha} \left(\frac{r_c}{r}\right)^2. \quad (93)$$

In writing this formula for  $\bar{\beta}_c$  we have also assumed  $r \gg r_0$  and have ignored the absorption corrections. This latter assumption is well founded in the limit  $r \gg r_0$ , as can be seen from the velocity surfaces in Figure 2. The rays labeled  $c'$  form a very small proportion of those rays originating on the core, and the proportion becomes vanishingly small as  $r/r_0 \rightarrow \infty$ .

Another useful asymptotic result is that for the normalization constant  $\eta$ . In order that the optical thickness  $\tau'$  be large at all depths, the more restrictive assumption  $\tau_0 \gg 1$  must be made. Then, the quantity  $1 - e^{-\tau'}$  is approximately unity for rays that intersect the surface and is equal to zero for those that do not, so that

$$\eta = \frac{1}{2} \int \frac{d\mu}{\tau}, \quad (94)$$

where the integral is over those angles for which intersections occur. This expression leads to the general result that

$$\eta \sim \frac{1}{2\tau_0} \left(\frac{r}{r_0}\right)^{1-2\alpha} \left[ \frac{4}{3(1+\alpha)^{1/2}} + \frac{1+\alpha}{3} (\mu_i^3 + \mu_R^3) - (\mu_i + \mu_R) \right], \quad (95)$$

where

$$\mu_i^2 = \frac{r^{2\alpha}(r_0^2 - r^2)}{r^{2\alpha+2} - r^{2\alpha+2}}, \quad \mu_R^2 = \frac{r^{2\alpha}(R^2 - r^2)}{R^{2\alpha+2} - r^{2\alpha+2}} \quad (96)$$

and  $\mu_i$  and  $\mu_R$  are taken as positive.

One application of these results is to derive the asymptotic behavior of the source function in the disconnected approximation. For simplicity we treat only the case  $\epsilon = 0$ . From equations (57), (92), and (93),

$$S_0 = \frac{\bar{\beta}_c}{\beta} I_c \sim A \left(\frac{r_0}{r}\right)^2, \quad (97)$$

where

$$\begin{aligned} A &= \frac{1}{4} \alpha \left[ \frac{4}{3(1+\alpha)^{1/2}} + \frac{1}{3} \alpha - \frac{2}{3} \right]^{-1} \\ &= 0.41019, \quad \alpha = 1 \\ &= 0.21234, \quad \alpha = \frac{1}{2}. \end{aligned} \quad (98)$$

Similarly, the above results lead to the following asymptotic expression for the source function in the GG approximation, again with  $\epsilon = 0$ :

$$S_{GG} \sim \left(\frac{r_c}{r}\right)^2 (I_c \alpha / 4) \left/ \left[ \frac{2}{3(1+\alpha)^{1/2}} + \frac{\alpha}{3} - \frac{2}{3} - \frac{1+\alpha}{6} (\mu_i^3 + \mu_R^3) + \frac{1}{2} (\mu_i + \mu_R) \right] \right. \quad (99)$$

### g) General Multiple Velocity Surfaces

We shall briefly consider problems with velocity surfaces of general multiplicity, say  $N$ . Before finding generalizations of equations (45) and (46), we need to introduce a more convenient notation for the various resonance points. Let the resonance point in question be labeled 1, and let the successive resonance points back along the ray be labeled 2, 3, ..., up to a maximum of  $N$ . It follows readily that

$$I_v^{\text{emg}} = I_v^{\text{inc}} \exp \left( - \sum_{i=1}^N \tau_i \right) + \sum_{j=1}^N S_j [1 - \exp(-\tau_j)] \exp \left( - \sum_{i=1}^{j-1} \tau_i \right). \quad (100)$$

If there are fewer than  $N$  such resonance points, we simply set the corresponding  $\tau$ 's equal to zero, in accordance with our previous convention. Equation (100) is the generalization of equation (45). The desired generalization of equation (46) can similarly be shown to be

$$I(r_1, n) = I_v^{\text{inc}} \frac{1 - \exp(-\tau_1)}{\tau_1} \exp\left(-\sum_{i=2}^N \tau_i\right) + \left[1 - \frac{1 - \exp(-\tau_1)}{\tau_1}\right] S_1 + \frac{1 - \exp(-\tau_1)}{\tau_1} \sum_{j=2}^N S_j [1 - \exp(-\tau_j)] \exp\left(-\sum_{i=2}^{j-1} \tau_i\right). \quad (101)$$

Let us integrate this over all solid angles to obtain

$$\bar{J}(r_1) = \bar{\beta}_c I_c + (1 - \beta) S(r_1) + \frac{1}{4\pi} \int d\Omega \frac{1 - \exp(-\tau_1)}{\tau_1} \sum_{j=2}^N [1 - \exp(-\tau_j)] \exp\left(-\sum_{i=2}^{j-1} \tau_i\right) S(r_j). \quad (102)$$

The quantity  $\beta$  is defined exactly as before in equation (34), while  $\bar{\beta}_c$  is now

$$\bar{\beta}_c = \frac{1}{4\pi} \int_{\Omega_c} d\Omega \exp\left(-\sum_{i=2}^N \tau_i\right) \frac{1 - \exp(-\tau_1)}{\tau_1}. \quad (103)$$

Equation (102) is of the same general form as equation (47), except that there are now corrections for absorptions in resonance regions lying between  $r_1$  and the location of the emission at points  $r_j$ . The quantity  $\bar{\beta}_c$  had previously contained one such correction factor, and now it contains  $N - 1$ . One consequence is that the construction of the kernel  $K(r, r')$  in cases of spherically symmetric flow will now depend on the detailed form of the CP surface, in contrast to the double-surface case.

However, our primary conclusion must be that the theory of the double-surface case has already encountered the major physical difficulty of the general case, namely, the nonlocal radiative coupling between all parts of the medium. We expect that, in cases of general multiplicity,  $\Lambda$ -iteration can continue to be used to advantage, as is the case for double surfaces. This would be an important result for the practical solution of these problems, and we hope to investigate this in future work.

### III. RESULTS AND DISCUSSION

Numerical work was limited to spherically symmetric models with inverse power-law velocity distributions with  $\alpha = 0.5$  and  $\alpha = 1.0$ . In addition to  $\alpha$ , each model is parametrized by  $\tau_0$ , defined by equation (87) and the ratio  $r_{\text{max}}/r_c$  of the outer radius to the inner radius.

#### a) Numerical Method

The integral equation (50), with the integral term in the form given by equation (68), is discretized by generating a preliminary radial grid in which the ratio of the length of successive intervals is  $(r_{\text{max}}/r_c)^{1/n}$ , where  $n$  is typically 10 to 60, and then halving each interval to obtain a final grid on which Simpson's rule can be used to evaluate the integral. This procedure is very convenient and in particular makes integration very rapid, but does introduce some error when the point at which the kernel has a discontinuous derivative lies at the midpoint of the Simpson formula. The functions  $\beta(r_i)$  and  $\bar{\beta}_c(r_i)$  are generated by numerical integration of equations (40) and (74), or by the use of asymptotic formulae, as appropriate, and the kernel is tabulated as a two-dimensional array. As a check on the accuracy of the kernel evaluation and the integration formulae, the normalization integrals for large values of  $\tau_0$  are evaluated and compared with equation (95). When the point at which the kernel has a discontinuous kernel coincided with the endpoint of the Simpson's formula, the agreement was essentially perfect; and when it coincided with a midpoint, the typical error was on the order of 1%. The resulting set of linear equations is then solved by iteration, starting with  $S_0(r)$  defined in equation (57) as the initial estimate. The maximum change in the solution is monitored and found to decrease by a factor of 3 to 10 on each iteration. Solutions have been obtained for cases with  $r_{\text{max}}/r_c$  in the range from 3 to  $10^6$ , with no sign of instability or impaired convergence. Typically we have used 20 radial points per decade; but because  $\beta_c$  and  $\beta$  (for  $\alpha \neq \frac{1}{2}$ ) decrease very rapidly for  $r \approx r_c$ , the use of a finer grid for the first decade might be advisable.

The emergent flux profiles are calculated by evaluating equation (45) at  $r = r_{\text{max}}$  and substituting the resulting expression for  $I(\nu, p)$  into equation (39). For a fixed value of  $\nu$  the form of this expression changes at a number of critical values of the impact parameter  $p$  determined by the core radius and the features of the velocity surface;  $I(\nu, p)$  can also be discontinuous at these critical values. A rather complex logical problem must be solved to enumerate and locate these critical values; between them the integrand is continuous, and an adaptive integration procedure based on Simpson's rule is used.

Evaluation of the flux profiles corresponding to  $S$  and  $S_0$  required roughly as much computer time as did the solution of the integral equation for  $S$ . Since the major part of the latter calculation was the evaluation of  $\bar{\beta}_c$ ,

the time required for the solution with a double surface was not much greater than with a single surface, although the amount of computer storage is substantially increased. Typically solving 15 cases with  $10 \leq r_{\max}/r_c \leq 10^3$  and evaluating and graphing both flux profiles required 5 minutes of central processor time on the CDC 6400.

*b) Comparison of Approximations*

The most important part of the discussion is the assessment of the importance of the radiative coupling of the surfaces, as expressed by the relative magnitude of the integral term in equation (50). Because this equation is potentially applicable to a number of astrophysical problems that involve a wide range of physical conditions, we have considered three basic cases characterized by the nature of the true sources and the probability per scattering  $\epsilon$  that a photon is absorbed:

I:  $I_c = 1, B = 0, \epsilon = 0, 10^{-4}, 0.5$  ;

II:  $I_c = 0, B = 1, \epsilon = 10^{-4}, 0.5$  ;

III:  $I_c = 0, B = r^{-2}, \epsilon = 10^{-4}, 0.5$  .

In each case we take  $\alpha = 0.5$  and  $1.0$ ,  $\log \tau_0 = -1(1)3$ , and  $\log (r_{\max}/r_c) = 1, 2, 3$ ; occasionally results for  $\log \tau_0 = 4$  have been computed as well. As the equation for the source function is linear, results for a combination of radiative and thermal excitation can be obtained by superposing the above cases.

The results are summarized in Table 1, which contains the maximum value of  $S/S_0$  and  $F(\nu_0)/F_0(\nu_0)$ ; as is obvious from the integral equation,  $S(r) \geq S_0(r)$  and  $F(\nu) \geq F_0(\nu)$ . For cases I and III,  $S/S_0$  is largest at or near

TABLE 1  
MAXIMUM VALUES OF  $S/S_0$  AND  $F(\nu_0)/F_0(\nu_0)$

$\epsilon$	$\log \tau_0$	$\alpha = 0.5$						$\alpha = 1.0$					
		$r_{\max} = 10$		$r_{\max} = 10^2$		$r_{\max} = 10^3$		$r_{\max} = 10$		$r_{\max} = 10^2$		$r_{\max} = 10^3$	
		$S/S_0$	$F(0)/F_0(0)$	$S/S_0$	$F(0)/F_0(0)$	$S/S_0$	$F(0)/F_0(0)$	$S/S_0$	$F(0)/F_0(0)$	$S/S_0$	$F(0)/F_0(0)$	$S/S_0$	$F(0)/F_0(0)$
CASE I													
0.0 . . . .	-1	1.12	1.01	1.26	1.03	1.42	1.06	1.34	1.07	3.44	1.72	12.5	3.89
	0	1.34	1.06	2.29	1.30	4.09	1.76	2.01	1.27	7.18	2.59	26.1	6.57
	$\geq 1$	1.34	1.07	2.43	1.35	4.78	1.95	2.11	1.29	7.56	2.68	27.5	6.81
0.0001 . .	-1	1.12	1.01	1.26	1.03	1.42	1.06	1.34	1.07	3.44	1.71	12.4	3.87
	0	1.34	1.06	1.91	1.30	4.09	1.76	2.01	1.27	7.15	2.58	25.1	6.23
	1	1.34	1.07	2.43	1.35	4.77	1.95	2.10	1.28	7.25	2.56	20.3	4.85
	2	1.34	1.06	2.40	1.34	4.68	1.93	2.04	1.26	3.21	2.03	9.12	2.48
	3	1.29	1.05	2.17	1.27	3.94	1.73	1.70	1.13	2.71	1.29	3.01	1.32
CASE II													
0.0001 . .	-1	1.08	1.04	1.12	1.05	1.13	1.08	1.25	1.09	2.35	1.12	6.95	1.13
	0	1.23	1.07	1.44	1.08	1.56	1.08	2.11	1.12	6.58	1.13	21.4	1.12
	1	1.23	1.06	1.48	1.07	1.65	1.07	2.53	1.12	8.65	1.12	21.0	1.08
	2	1.22	1.06	1.47	1.07	1.63	1.07	2.40	1.11	5.84	1.08	7.79	1.02
	3	1.19	1.05	1.40	1.06	1.52	1.06	1.79	1.07	2.39	1.02	2.49	1.00
	4	1.08	1.02	1.15	1.02	1.16	1.02	...	...	...	...	...	...
0.5 . . . .	-1	1.04	1.02	1.05	1.02	1.06	1.02	1.09	1.03	1.18	1.02	1.20	1.00
	0	1.06	1.02	1.11	1.02	1.13	1.02	1.12	1.01	1.15	1.00	1.15	1.00
	>1	1.01	1.00	1.02	1.00	1.03	1.00	1.02	1.00	1.02	1.00	1.02	1.00
CASE III													
0.0001 . .	-1	1.13	1.08	1.27	1.15	1.43	1.22	1.26	1.20	1.56	1.52	1.78	1.71
	0	1.47	1.19	2.63	1.62	4.74	2.30	1.38	1.32	1.67	1.61	1.82	1.73
	1	1.47	1.17	2.91	1.67	5.78	2.59	1.39	1.31	1.65	1.59	1.73	1.59
	2	1.47	1.17	2.87	1.65	5.65	2.51	1.36	1.29	1.52	1.45	1.53	1.34
	3	1.40	1.14	2.56	1.55	4.69	2.23	1.23	1.19	1.26	1.20	1.26	1.14
	4	1.17	1.06	1.57	1.21	2.13	1.43	...	...	...	...	...	...
0.05 . . . .	-1	1.06	1.04	1.12	1.07	1.11	1.10	1.09	1.07	1.13	1.10	1.13	1.08
	0	1.13	1.05	1.38	1.16	1.69	1.29	1.05	1.05	1.06	1.04	1.06	1.03
	1	1.02	1.01	1.08	1.03	1.14	1.06	1.00	1.00	1.01	1.00	1.01	1.00
	>2	1.00	1.00	1.01	1.00	1.01	1.01	...	...	...	...	...	...

TABLE 2  
COMPARISON OF GRACHEV AND GRININ'S APPROXIMATION  
( $I_c = 1$ ,  $B = \epsilon = 0$ ,  $r_{\max} = 100$ )

$\tau_0$	$\log r$	$\alpha = 0.5$			$\alpha = 1.0$		
		$S_{GG}$	$S_0$	$S_{\text{num}}$	$S_{GG}$	$S_0$	$S_{\text{num}}$
10.....	0.0	7.6-1	5.0-1	5.0-1	7.9-1	5.0-1	5.2-1
	0.5	2.4-2	1.6-2	1.9-2	6.2-2	3.5-2	4.7-2
	1.0	3.1-3	2.3-3	3.2-3	6.9-3	4.0-3	8.9-2
	1.5	2.8-4	2.4-4	4.3-4	5.6-4	4.1-4	1.7-3
	2.0	2.6-5	2.5-5	5.7-4	4.6-5	4.1-5	2.9-4
100.....	0.0	8.0-1	5.0-1	5.0-1	8.0-1	5.0-1	5.2-1
	0.5	1.9-2	1.3-2	1.5-2	6.2-2	3.5-2	4.8-2
	1.0	2.5-3	1.9-3	2.6-3	6.9-3	4.0-3	9.3-3
	1.5	2.3-4	2.1-4	3.7-4	5.6-4	4.1-4	1.7-3
	2.0	2.2-5	2.1-5	5.1-5	4.6-5	4.1-5	3.1-4

the outer boundary. Although  $F(\nu)/F_0(\nu)$  does not necessarily have its maximum value at  $\nu = \nu_0$ , the values of this ratio at  $\nu = \nu_0$  seem to be most appropriate for our purpose because the flux always peaks there. It is clear that the effect of the coupling increases with both  $r_{\max}$  and  $\tau_0$ , although in some cases it decreases for large  $\tau_0$  because of thermalization. Usually, but not always, the effect of coupling is larger for velocity laws with  $\alpha = 1.0$  than for those with  $\alpha = 0.5$ . Most of the observed effects can be explained in terms of the competition between escape processes, represented by  $\beta$ , and absorption processes, represented by  $\epsilon$ . For case II with  $\epsilon = 10^{-4}$  and  $\alpha = 1.0$ , the ratio  $F(\nu)/F_0(\nu)$  can be much larger (factor  $\sim 20$ ) than its value at line center. This case is remarkable among those that we have studied in that the source function increases strongly from the inner boundary to the outer (because  $\beta$  decreases), leading to extraordinarily narrow intense lines, which increase near line center by several orders of magnitude for a frequency change as small as  $0.01\nu_0$ . In this case, as in others, coupling reduces the magnitude of the slope of the source function. In the corresponding case with  $\alpha = 0.5$ , for which  $\beta(r)$  and therefore  $S_0(r)$  is constant, the source function either falls slowly and monotonically from the inner boundary to the outer, or increases very slightly before falling and  $F(\nu)$  exceeds  $F_0(\nu)$  by at most 60% away from the line center.

The approximation of Grachev and Grinin (1975) to the source function given by equation (58) is compared with both  $S_0$  and  $S$  in Table 2, for a selection of cases. For purely radiative excitation ( $B = 0$ ),  $S_{GG}$  exceeds the numerical value by a substantial amount; at larger radii,  $S_{GG}$  approaches  $S_0$  and is thus too small. Thus the approximation of Grachev and Grinin in these cases introduces a larger error overall than simply ignoring the coupling term. On the other hand, when  $B = \text{const.}$ ,  $S$  varies slowly with  $r$ ; and for  $\epsilon = 10^{-4}$  and  $\alpha = 0.5$ , the approximation is in error by 8% at most.

### c) Source Functions, Flux Profiles, and Radiation Force

It is now well known that for rapidly moving atmospheres the emergent spectra are generally very much more complex and show more variety of form than do the corresponding source functions. In particular, the effects of the velocity field enter much more strongly into the calculation of the flux profile than into the determination of the source function, primarily through the location of the velocity surface. In examining the numerical results below, we hope to make clear the general features of the radiation field and its dependence on the various parameters, and to illustrate the variety of possible profiles that can be obtained. No attempt is made to apply these results to the interpretation of particular astrophysical objects.

The *qualitative* features of the source function are apparent from the expression (51) for  $S_0$ . The terms in the numerator represent the sources of line photons arising from stellar radiation and thermal sources, respectively, while the terms in the denominator correspond to sinks in the form of thermal de-excitation and escape. If  $1 > \beta \gg \epsilon$  for all  $r$ , then  $S$  depends on  $\epsilon$  only through the source term; and if the excitation is primarily radiative,  $S$  becomes independent of  $\epsilon$ . On the other hand, if  $\tau_0$  is small, one can have  $\beta \gg \epsilon$  with the result that  $S$  is independent of  $\epsilon$ , while for large  $\tau_0$ ,  $\beta$  can fall below  $\epsilon$ , allowing  $S$  to depend sensitively on  $\epsilon$ . Because  $\beta$  is independent of  $r$  for  $\alpha = 0.5$ , and decreases strongly with  $r$  for  $\alpha = 1$ , the radiation field can be sensitive to  $\epsilon$  for one choice of velocity law, and insensitive to  $\epsilon$  for another. This situation is displayed clearly by Figure 4, where the radial dependence of  $\beta$  is given by the broken line. For thermal excitation at a constant temperature,  $S$  can actually increase outward because  $\beta$  decreases if  $\alpha \neq 0.5$ . On the other hand, for radiative excitation alone and strong absorption,  $S$  will be very much smaller than  $I_c$  if  $\tau_0 > 1$ ; the peculiarities of the emergent flux in this case are discussed below.

It appears from the numerical results that the source function within the atmosphere can be quite insensitive to the values of the outer radius. For example, in the case of purely radiative excitation with  $\epsilon = 0$ , increasing the outer radius by a factor of 10 causes the source function to decrease by at most 4% for  $\alpha = \frac{1}{2}$ , while for  $\alpha = 1$ ,

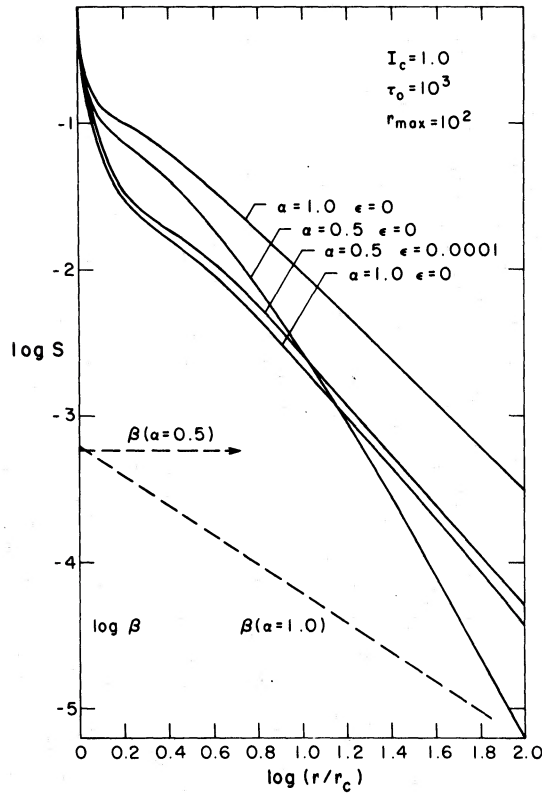


FIG. 4.—Source functions for various models with purely radiative excitation, showing effects of nonzero  $\epsilon$  and different velocity laws. Broken lines show behavior of  $\beta(r)$  for indicated values of  $\alpha$ .

the corresponding amount is approximately 20% for  $\tau_0 = 1$  and 10% for larger  $\tau_0$ . When  $\epsilon$  is increased to  $10^{-4}$ , these values become even smaller. In other words, for radiative excitation the source function depends very little on material at larger radii, even when  $S$  and  $S_0$  are quite different. In contrast, for  $B = 1$  and  $\epsilon = 10^{-4}$ , the source function increases rapidly with both  $\tau_0$  and  $r_{max}$ , because of the dominant effect of the real sources at radii larger than the one in question. It is curious that for  $\alpha = 0.5$ ,  $S(r = r_{max})$  is found numerically to be independent of the values of  $r_{max}$ .

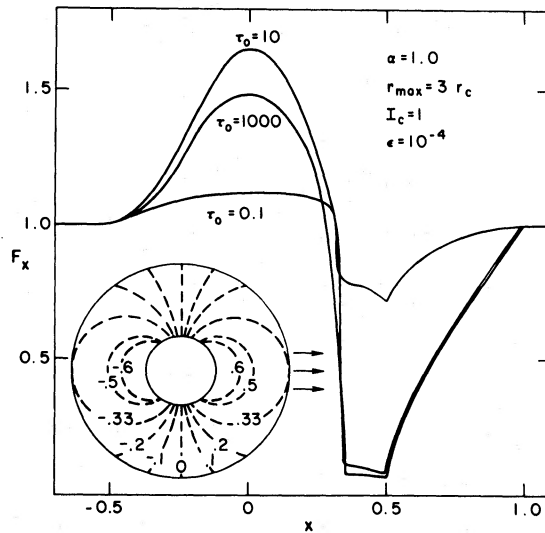


FIG. 5.—Flux profiles for various values of the parameter  $\tau_0$ , for  $r_{max}/r_c = 3$ . Inset shows location of CD velocity surfaces for indicated value of frequency displacement  $x$ .

We turn now to the behavior of the flux profile. For definiteness we plot the flux as a function of the frequency displacement in units corresponding to  $v_0$ :

$$F_x = 2 \int_0^{r_{\max}} I(x, p) p dp, \quad (104)$$

where

$$x = (v - v_0)/v_0(v_0/c). \quad (105)$$

The normalization chosen here is such that  $F_x = I_c$  for frequencies in the continuum ( $|x| > 1$ ). The general features of the profiles can be understood by reference to the insert of Figure 5, which shows the location of the CD surfaces for the indicated values of the frequency  $x$  in the case  $\alpha = 1.0$ ,  $r_{\max} = 3.0$ . The corresponding profiles (for radiative excitation with  $\epsilon = 10^{-4}$  and the indicated values of  $\tau_0$ ) appear in the body of Figure 5. For large negative values of  $x$ , the surface is completely occulted by the star, and only the stellar continuum is observed. As  $x$  increases, the surface emerges and its emission contributes to the flux, until  $x$  is equal to 0, when emission from the entire surface is seen. For small positive values of  $x$ , the projection of the surface on the plane of the sky shrinks rapidly. Because the surface is scattering the stellar radiation out of the line of sight, the flux falls until the surface becomes tangent with the outer boundary. As  $x$  increases, the flux remains low until the projection of the surface is smaller than the core, after which the stellar radiation emerges with increasing strength. The parts of the surface near the outer boundary move very rapidly as  $x$  varies near  $x = 0$ , so that if the source function is not too small near the outer boundary, the flux peak can be both very intense and extremely narrow. This effect increases strongly with  $r_{\max}$ , as is clear from Figure 6. One should be aware, however, that the dramatic behavior of the peak flux in Figure 6 depends mostly on the material at large radii, when the Sobolev approximation is most likely to fail because of the smaller velocity gradient.

The flux profiles corresponding to the source functions of Figure 4 as shown in the first two panels of Figure 7, along with the corresponding profile for the case of thermal excitation with  $B = r^{-2}$  and  $\epsilon = 10^{-4}$ , which appear in the third panel. The effect of the nonzero value of  $\epsilon$  is to reduce the peak intensity dramatically for  $\alpha = 1.0$  and moderately for  $\alpha = 0.5$ ; this sensitivity of the profile to  $\epsilon$  for critical cases should be borne in mind in modeling real systems. The thermal profiles appearing in the third panel are similar to those in the first two, except

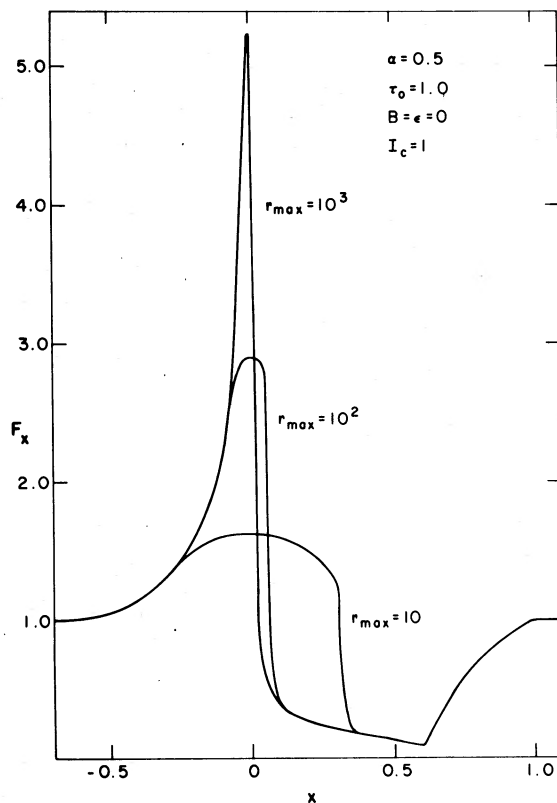


FIG. 6.—Flux profiles for various values of  $r_{\max}$

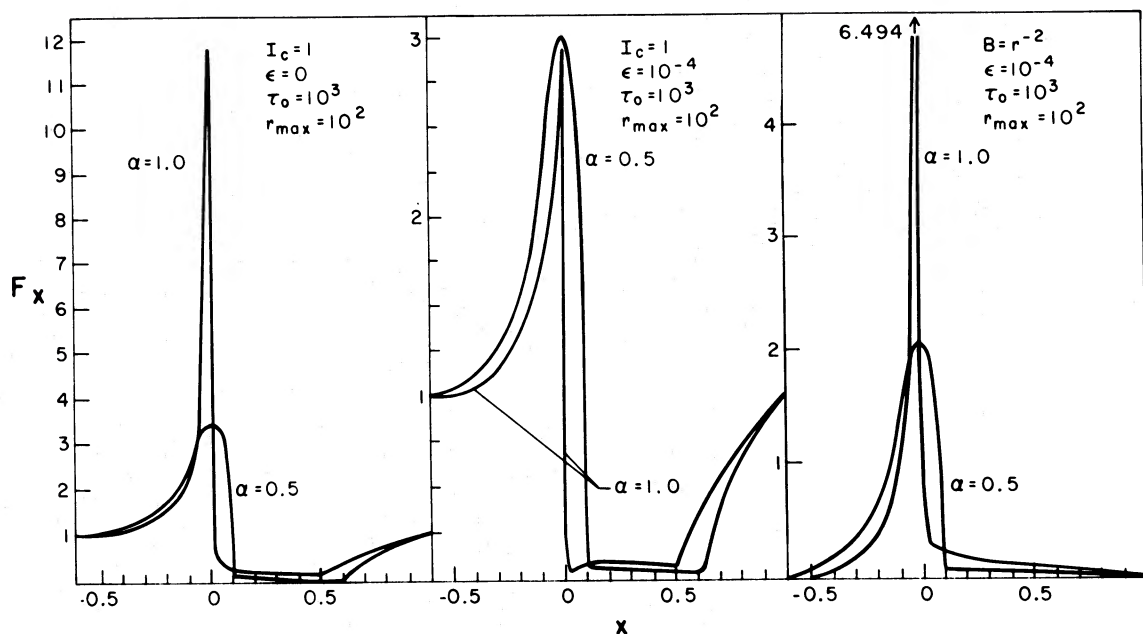


FIG. 7.—Flux profiles for radiative excitation with  $\epsilon = 0$  and  $10^{-4}$ , and for thermal excitation with  $B = r^{-2}$ , for both velocity laws.

that no absorption features are present. It is important to notice that the width of the peak gives no indication of the maximum flow speed  $v_0$ ; on the other hand, the extreme blue edge of the absorption feature remains a good indication of  $v_0$ .

It seems important to stress that the velocity laws of the type considered here can also produce very strong absorption features with little or no accompanying emission. Figure 8 shows the flux profiles for some radiatively excited cases in which the atoms have a large probability of being collisionally de-excited. As  $\tau_0$  becomes large, the atmosphere effectively absorbs all radiation for positive values of  $x$ , for which the velocity surface lies mainly between the star and the observer.

The force of radiation  $\bar{H}$ , as given by equation (71), is graphed in Figure 9 for the source functions appearing in Figure 4. The quantity  $\bar{H}$  is markedly less sensitive to the value of  $\epsilon$  than is the corresponding source function.

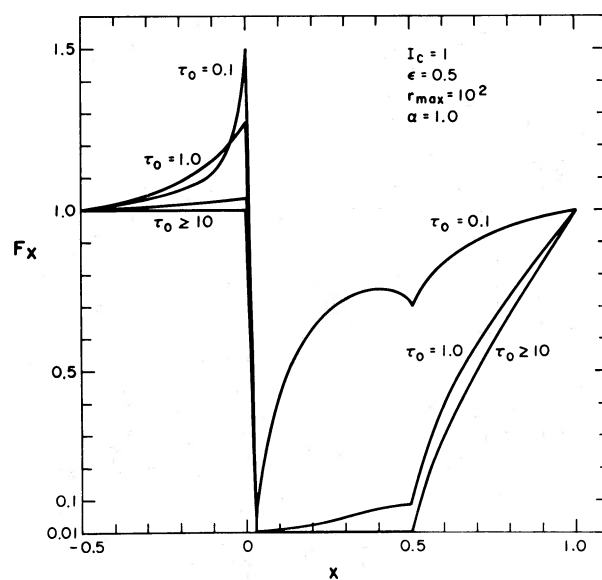


FIG. 8.—Flux profiles for pure radiative excitation and a high probability per scattering of collisional deexcitation

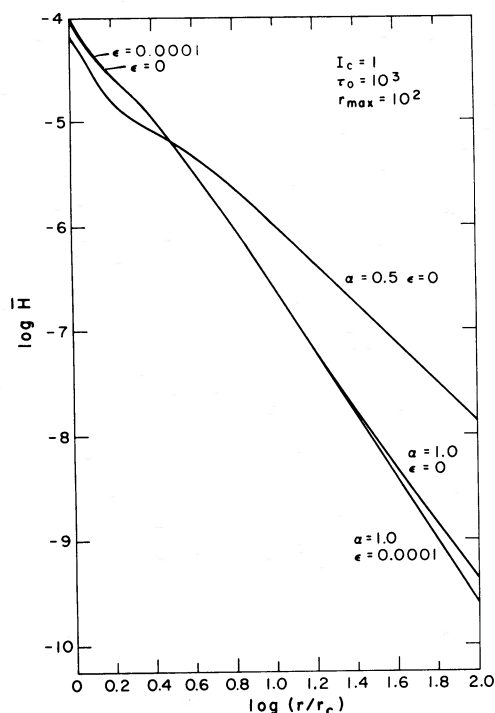


FIG. 9.—Radiation force  $\bar{H}$  for source functions shown in Fig. 4

For pure radiative excitation, the force of radiation is smaller than the value computed from  $S_0$  by 10–30% deep in the atmosphere and is larger by a few percent in the outer layers. When thermal sources are present, their contribution to  $\bar{H}$  is qualitatively different from that of radiative excitation. Near the inner boundary the force is directed inward—i.e.,  $\bar{H}$  becomes negative—while at larger radii the force is directed outward. Because the radiative contribution to the force falls off so rapidly as the radius increases, it is essential that the thermal contribution be included in any discussion of radiation force in specific astrophysical objects.

We wish to thank Drs. Felix Marti and Peter Noerdlinger for a preprint of their paper. This work was supported in part by the National Science Foundation through grant AST 76-22032.

#### REFERENCES

- Batchelor, G. K. 1967, *An Introduction to Fluid Mechanics* (Cambridge: Cambridge University Press).
- Castor, J. I. 1970, *M.N.R.A.S.*, **149**, 111.
- . 1974, *M.N.R.A.S.*, **169**, 279.
- de Jong, T., Chu, S.-I., and Dalgarno, A. 1975, *Ap. J.*, **199**, 69.
- Grachev, S. I., and Grinin, V. P. 1975, *Astrophysics*, **11**, 20.
- Hummer, D. G. 1976, in *Be and Shell Stars*, ed. A. Slettebak (Dordrecht: Reidel).
- Hummer, D. G., and Rybicki, G. B. 1971, *Ann. Rev. Astr. Ap.*, **9**, 237.
- Kuan, P., and Kuhi, L. V. 1975, *Ap. J.*, **199**, 148.
- Lucy, L. B. 1971, *Ap. J.*, **163**, 95.
- Marti, F., and Noerdlinger, P. D. 1977, *Ap. J.*, **215**, 247.
- Mihalas, D., Kunasz, P. B., and Hummer, D. G. 1975, *Ap. J.*, **202**, 465.
- Mihalas, D., Kunasz, P. B., and Hummer, D. G. 1976a, *Ap. J.*, **203**, 647.
- . 1976b, *Ap. J.*, **206**, 515.
- . 1976c, *Ap. J.*, **210**, 419.
- Noerdlinger, P. D., and Rybicki, G. B. 1974, *Ap. J.*, **193**, 651.
- Rybicki, G. B. 1970, in *Spectrum Formation in Stars with Steady-State Extended Atmospheres*, ed. H. Groth and P. Wellmann, NBS Spec. Publ. No. 332 (Washington: U.S. Government Printing Office), p. 87.
- Sobolev, V. V. 1947, *Moving Envelopes of Stars* (Leningrad: Leningrad State University [in Russian]); English transl. S. Gaposchkin (Cambridge: Harvard University Press, 1960).
- . 1957, *Soviet Astr.—AJ*, **1**, 678.

*Note added in proof.*—Efficient algorithms for the generation of the functions  $\beta$ ,  $\beta_c$ , and  $\gamma_c$  have been developed; an account of this work will be published elsewhere.

D. G. HUMMER: Joint Institute for Laboratory Astrophysics, University of Colorado, Boulder, CO 80309

G. B. RYBICKI: Smithsonian Astrophysical Observatory, 60 Garden Street, Cambridge, MA 02138